SrO assisted 1393 glass scaffold with enhanced biological compatibility

6.1 INTRODUCTION

Bioactive glasses are biodegradable materials that convert to bone minerals in physiological fluid. It could be utilized to design three dimensional porous scaffold or biopolymeric composite matrices through foam replica technique, freeze drying, electrospinning, 3D printing etc., and further utilized to generate tissue engineered constructs for bone tissue engineering applications (Baino et al., 2019, Singh et al., 2020). Due to biocompatibility, the bioactive glass derived scaffolds allow hard tissues (angiogenesis) to grow inside the 3D interconnected porous struts by means of osteoconduction and osseointegration. Further, the therapeutic ions incorporated 3D porous bioactive scaffolds promote the new bones and blood vessels formation by stimulating osteogenesis and angiogenesis, and facilitate cell-scaffolds attachments, and eventually reconstruct the damaged or diseased bones (Singh et al., 2020). The bone tissue growth and anchorage on bioactive glass scaffolds are characterized by osteoconduction (a phenomenon through which the newly formed bones can migrate into biocompatible porous struts), followed by osseointegration (a stable anchorage of that migrated bones with the porous scaffolds achieved through bone-alike direct bone-scaffold bonds). (Albrektsson and Johansson, 2001).

Strontium along with calcium and phosphate and at least dozens of other elements forms hydroxyapatite (HAp; $Ca_{10}(PO_4)_6(OH)_2$), the mineral component of bone (Pilmane et al., 2017, Gomes et al., 2019). Strontium is one of the most essential elements that plays a pivotal role in contributing healthy bone formation, bone metabolism, increase bone

mineral density, active osteoblasts formation and prevents osteoclasts mediated bone resorption, thereby regulates overall health of the bones (Gentleman et al., 2010, Kargozar et al., 2019, Baier et al., 2013). Strontium has earlier been reported as having the potential to prevent or lessen osteoclastogenesys, a process through which osteoclasts develop from haemopoietic cells of the monocyte-macrophage cell lineage and subsequent bone resorption (Gentleman et al., 2010, Choi et al., 2016). Like calcium, strontium is also an indispensable element present naturally in nearly every food we take in our daily diet (Melnyk et al., 2019). Even, strontium has earlier been used as supplements in the form of strontium renalate (SrRAN, Protelos®) to increase bone density, cure osteoporosis and prevent bone loss until its intake was reported responsible for rising cardiovascular diseases (Cianferotti et al., 2013, Doublier et al., 2011, Ruiz et al., 2009, Nitiputri, 2015, Marie, 2005, Marie, 2006). In 2014, with the European Medicines Agency's Pharmacovigilance Risk Assessment Committee (PRAC) recommendation, the European Union had withdrawn Protelos®/Osseor from use to treat osteoporosis due to serious negative side effects, including cardiovascular diseases, excessive bone growth, and even increased osteoporosis. Although seeming contrasting, yet the increase in osteoporosis or cardiovascular diseases in many cases, could be due to excessive SrRAN intake, digestion inability and other contraindications (i.e. hypertension, ischemic cardiovascular disease, cerebrovascular disease, peripheral arterial disease etc.) (Maria et al., 2017, Reginster et al., 2015, Reginster, 2014). It is worth mentioning that, in 2019, the use of SrRAN drug has been permitted again in the UK to treat severe osteoporosis, especially in postmenopausal women who are at high risk of fracture (Dr. Nicola Peel, the clinical adviser for the National Osteoporosis Society, welcomed the decision). However, other forms of strontium (strontium citrate or chloride) are reported to be used till date as bone supplements but

without FDA's approval. Whatsoever, the strontium in the 1393 bioactive glasses is different from the SrRAN (Protelos®/Osseor®). Nevertheless, in this investigation, the SrO derived macroporous 1393 glass scaffolds (% AP >50%) mimicking the trabecular bones were prepared by 'partial to complete' substitution of CaO by SrO to examine physicomechanical, and biological effects. However, the strontium incorporated bioactive glasses/ glass derived scaffolds need more comprehensive studies (in vitro, in vivo, and ex vivo) prior clinical trials.

.6.2 MATERIALS AND METHODS

6.4.1 Scaffold and SBF preparation

The 1393 glass derived scaffolds were synthesized via wet-chemical sol-gel route through stepwise hydrolysis of precursors. Briefly, required amount of 1(M) HNO_3 was added with proportionate amount of TEOS (Tetraethoxysilane; assay 98%, Sigma-Aldrich, IN), TEP (Triethyl phosphate assay 99%, Sigma-Aldrich, IN), $Mg(NO)_3$, $Ca(NO)_3.4H_2O$, KNO_3, $NaNO_3$ and $Sr(NO_3)_2$ (Assay >99%, Loba chemie, IN) one after another in sequence maintaining 45 min gap in each step allowing complete hydrolysis of the precursors. The molar ratio of $(H_2O+HNO_3)/$ $(TEOS+TEP)$ in the whole processes was maintained at 9. 1-5 vol% of PVA was added to the solution prior polyurethane foams of $2\times10\times10mm^3$, $10\times10\times10mm^3$ and $25\times10\times10mm^3$ were dipped into the sols as soon as the thickening of the gelling starts. The resultant sols were then kept for aging for at least 48h in ambient temperature to convert into gels. The gel infiltrated foams then were carefully taken out, excess gel from the foam was cut out and then allowed to dry for additional 48h at 70-80 ˚C in a control heating oven (IKON, IN). The gel-infiltrated foams were then burnt out by heat-treating the foams upto 800 ˚C in a control heat furnace. In a two-step heating, beginning with 5 ˚C/min up to 300 ˚C and then holding for 2h, and then heating again at

0.5 ˚C/min up to 800 ˚C and holding for 6h, followed by a slow cooling (2 ˚C/min) the binder and foams were burnt out and foam replicated scaffolds were prepared.

Table 6.1: Percentage (mol %) in chemical compositions of the SrO derived 1393 scaffold

Chemical compositions	S1	S2	S3	S4	S5
SiO2	54.65	54.65	54.65	54.65	54.65
CaO	22	20.9	17.6	11	0
Na2O	6	6	6	6	6
K2O	7.9	7.9	7.9	7.9	7.9
MgO	7.7	7.7	7.7	7.7	7.7
P2O5	1.75	1.75	1.75	1.75	1.75
SrO	0	1.1	4.4	11	22

The SBF preparation has been described briefly in chapter 4.

6.2.2 Assessment of bioactivity

In vitro bioactivity of the 'soaked at 10mg/ml in SBF' glass derived samples (powder & scaffold constructs) for particular days were evaluated through XRD, SEM-EDX, FTIR and pH analysis. The fine enough powdered scaffolds were characterized through Ni filtered Cu-K$_\alpha$ sourced RIGAKU Miniflex II, X-ray diffractometer with having tube voltage of 40 kV and current of 20 mA over the angular range (2θ) of 10-80˚ and scan rate of 3˚ min^{-1}. Peaks were identified using International Centre for diffraction Data (ICDD) cards. Physico-chemical behavior of the SBF solution to which the glass samples were soaked in was measured at particular intervals using Universal Bio microprocessor digital pH meter (India). The molecular functional groups of the derived scaffolds were identified using Fourier Transform Infrared Spectrometer BRUKER Tensor 27 (Germany) taking 32 scans with resolution of 4 cm^{-1} in transmittance mode within the frequency range of 4000- 400 cm^{-1}. The microstructural morphology of the SBF treated scaffold constructs assuring HAp

nodules formation was examined using EVO|18, SEM (ZEISS, US). The scaffold constructs were gold coated for 150 sec with and were analyzed through SEM-EDX. Energy Dispersive X-ray spectroscopy, operating at 20 keV EHT was used to scan over the scaffold constructs to determine the elemental atomic % on the scaffolds surfaces. Ca/P ratio was estimated from the elemental atomic % and correlated with the stoichiometric calcium+strontium/phosphorous ratio of bone minerals for assurance of HA like layer formation.

6.2.3 Biocompatibility of the scaffolds

Mouse fibroblast L929 cell lines from NCCS (National Center for Cell Science, INDIA) were used for *In vitro* cytocompatibility of the glass derived scaffolds. The L929 cells were cultured into complete culture media with 10% FBS, supplemented with 100 U/ml penicillin-streptomycin, 5% CO_2 and 95% humidified atmosphere at 37 ˚C. Upon attaining 70% cells confluence, the cell culture plates were treated with 0.25% trypsin in 95% humidity and 5% CO_2 atmosphere at 37 ˚C. Trypsinized cells were centrifuged at 300g for 10 min and re-suspended. The pellets were washed twice with PBS. Scaffold constructs (S1, S2, S3 and S5) were sterilized upon ethanol/UV treatments succeeding incubation at 37 ˚C for 2h in complete culture media in 5% CO_2 and 95% humidified environment. Finally, the cytological compatibility assessments of the scaffolds were examined using the obtained cells.

Cellular viability, cell lysis, metabolic activity and adhesion of cells on scaffold constructs were analyzed using Calcein AM and Ethidium homodimer-1 staining, MTT (3-(4,5-dimethylthiazol-2-yl)-2,5-diphenyltetrazolium bromide) assay and scanning electron microscopy EVO|18, SEM (ZEISS, US). The suspended cells (1×10^5 cells / cm^2) in culture media were seeded onto the scaffold construct and were cultured for a predetermined period in 5% CO_2, 95% humid atmosphere at 37 ˚C. Scaffolds on a certain interval were washed with PBS and incubated with 100µl of fresh media and 10µl of MTT (5mg/ml) reagent for 2h. In succession, the formazan crystals were solubilize by mixing of 100µl of solubilization solution. The absorbance was recorded at 570 nm. The live (green) and dead (red) cells after growing onto scaffolds constructs for 24h and incubated in Calcein AM

and Ethidium homodimer-1 staining solution for 30-40 min were detected using fluorescence microscopy (Olympus BX51, Japan).

6.2.4 Mechanical properties

The as prepared scaffolds of various dimensions ($25\times10\times10mm^3$ and $10\times10\times10mm^3$) were brought under universal testing machine (UTM) H10KL (Tinius olsen, US) for measurements of compression and flexural stress and flexural modulus of the scaffolds. Mechanical properties of the scaffolds were measured in accordance with the standard protocol ASTM C1674-11, maintaining crosshead speed of 0.5mm/min under the uniaxial 10KN load cell. The compressive (σ_c) and flexural (σ_f) stress and elastic modulii of flexure (E_f) were calculated using the formulae described in chapter 4.

Porosities (AP) of the scaffolds were determined using solvent saturation method in methanol as follows. Briefly the weights of the porous scaffolds after dipping into methanol (solvent) were monitored until constant weights were achieved.

6.3 Statistical analysis

Unpaired student's t-test or one way ANOVA followed by Tukey's post hoc test was performed while comparing between pairs/groups. Experiments were performed in triplicates and the data were presented as mean ± standard deviation (SD). Differences were considered significant for 'p' value less than 0.05 (*) or 0.01(**) and 0.001(***).

6.4 RESULTS

6.4.1 In vitro bioactivity: Structural, morphological, functional and physico-chemical evaluation

Bioactivity of materials confirmed through characteristic changes in structural, functional, morphological and physico-chemical properties. In this investigation, we have characterized the scaffolds and/or powder by XRD, SEM-EDX, FTIR and pH to assess the in vitro bioactivity by means of structural and morphological modifications and alterations in functional and chemical behavior. Herein, by the structural characterizations of glass-derived scaffolds, some definite alterations in peaks properties and intensities of the soaked in SBF samples comparing the sintered only scaffold have been noticed. By the XRD diffractograms (Fig 6.1) we observed several moderate to intensely modified peaks for the soaked glass sample over the angular range (2θ) of 20-70 ˚. However, the major modifications in spectral intensities were appeared particularly at the angular position 32˚, 45˚ and 56˚. Several other mild to moderate peaks were also appeared at various spectral values.
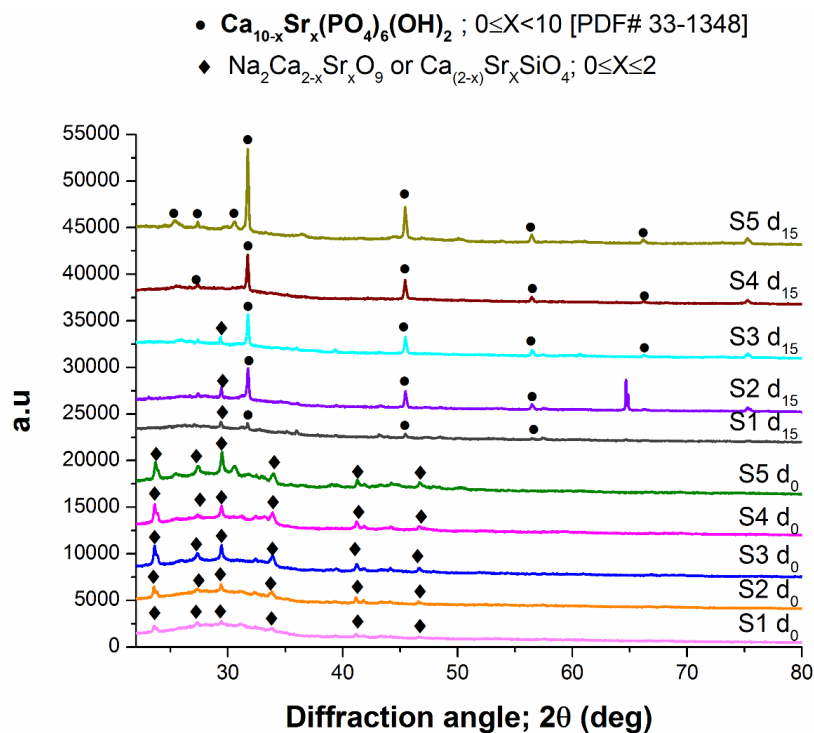

Fig 6.1 XRD analysis of 'soaked in SBF for 15days' (above five curves) and as prepared (sintered only) samples. Post SBF treated samples showing formation of HCA layer after 15 days of incubation in SBF.

Functional groups responsible for HAp like nodules formation were examined by the characteristic resonances in FTIR spectra over the frequency range of 4000-400 cm^{-1}. In the IR region (4000-400 cm^{-1}) the molecules or phases of a compound containing particular bond energy either vibrate or rotate by absorbing same amount of energy from the IR radiation and yield spectrums as a result (Stuart, 2000). The IR spectral resonances observed at lower wave number (400-700 cm^{-1}) can be attributed due to the bending vibrations of atoms in molecules, as the stretching vibrations generally appear at relatively higher wavenumbers due to the fact that, stretching vibrations require change in bond length. However, in this investigations (Fig 6.2), the main characteristic bands pertaining to particular phases appeared at 450 cm^{-1}, 470 cm^{-1}, 550-640 cm^{-1}, 670 cm^{-1}, 760 cm^{-1} were originated mainly from bending vibrations of atoms in PO$_4$ tetrahedron. Furthermore, the resonance at 1040 cm^{-1} which became intense over time (i.e. for the soaked samples) was ascribed to the symmetric stretching of P-O bands(Rezaei et al., 2014, Ali et al., 2019). Moreover, the resonances over 1100-1700 cm^{-1} and 2700-3700 cm^{-1} were attributed mainly due to the presence of carbonyl and hydroxyl groups in the glass samples.
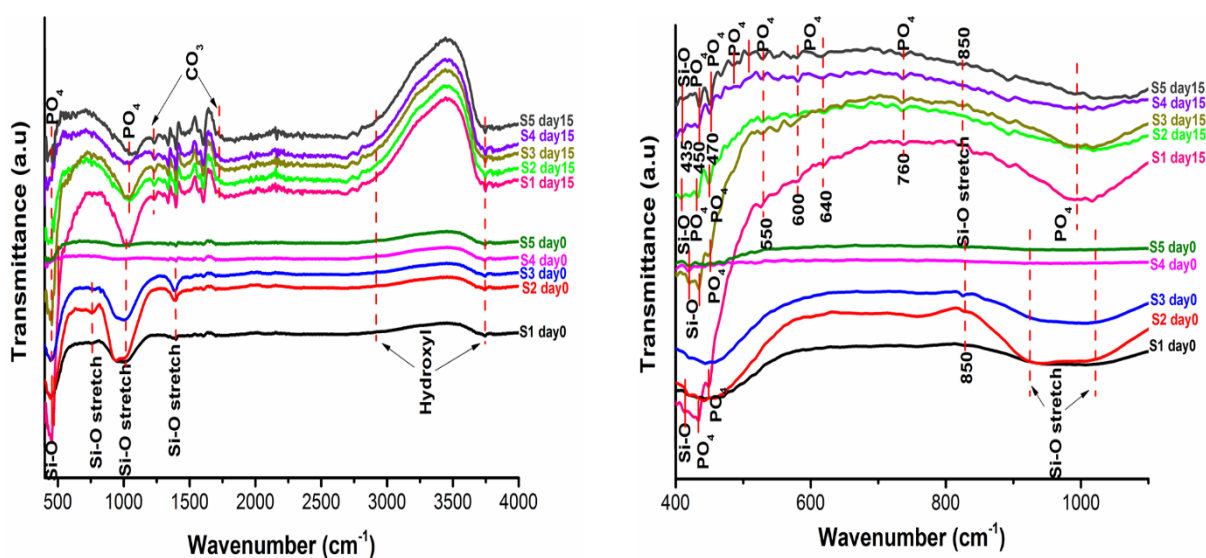

Fig 6.2 FTIR spectral resonances of the soaked in SBF (above) and pretreated samples showing characteristics functional bands (PO$_4$) corresponding to HCA layer formation for the soaked in samples

The pH behavior of the SBF solutions onto which the glass samples were kept for soaking were examined on particular intervals. The results (Fig 6.3A) demonstrate that the pH values were kept increasing upto the initial 5 days and then decreased thereafter. The steepest increase as well as highest pH value, both were observed in S5 scaffold. The increase in SrO substitution for CaO in the glass system was appeared to have increased in pH of SBF solutions. Moreover, the highest and least pH value on day5 was observed in S5 (8.22 ± 0.5; n=3) and S1 (8.07± 0.5; n=3) respectively.

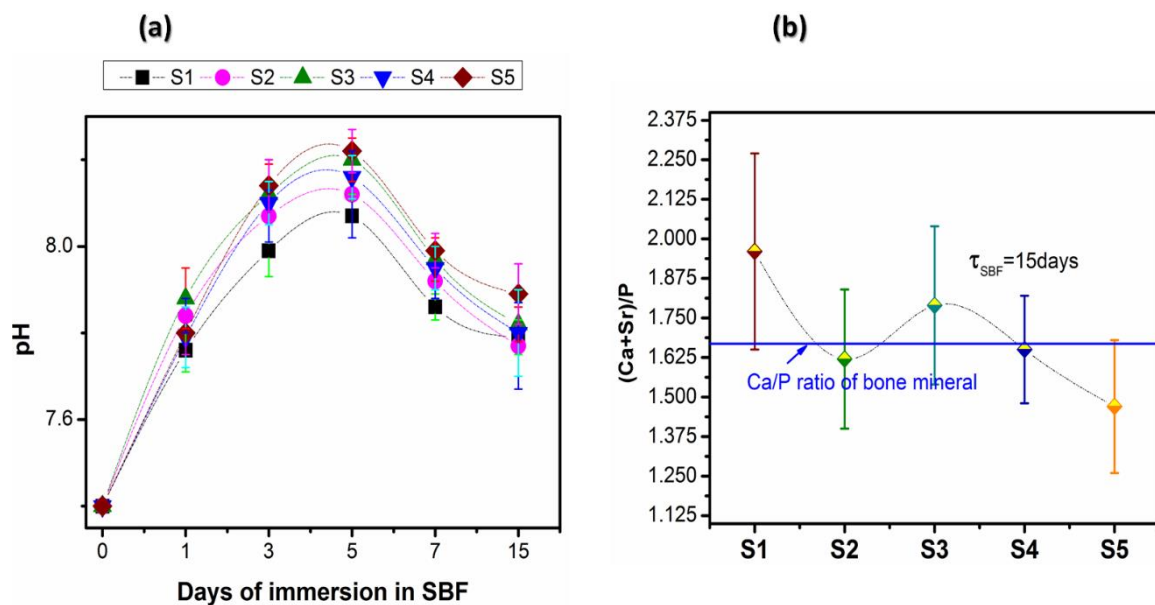**Fig 6.3** (**A**) pH as a function of materials' immersion time . (**B**) EDX obtained Elemental analysis to deduce quantitative Ca/P ratio as an indication of bioactivity of the materials.

Surface morphologies of the post SBF treated scaffolds for evolution of HAp like nodules were examined by Scanning Electron Microscopy. Results (Fig 6.4) demonstrate that heterogeneous clusters of nodules in the form of agglomerates, nano rods or flower alike granular particles were developed throughout the scaffolds' surfaces. The formation of

HAp nodules was appeared to have augmented in SrO modified scaffolds, except S5. The EDX analysis further reassures the HAp like layer formation on the surface of the scaffold constructs. The Ca/P ratios (Fig 6.3B) from the Energy Dispersive X-ray spectroscopic elemental presence (Atomic %) on the scaffolds surface were calculated and found similar to the stoichiometric ratio of bone mineral (1.67). The (Ca+Sr)/P ratios (*Table 6.2*) of the soaked samples (1.96 ± 0.17 in S1, 1.62 ± 0.21 in S2, 1.79 ± 0.14 in S3, 1.65 ± 0.14 in S4 and 1.47 ± 0.13 in S5) (n=3) were found nearly close to the Ca/P ratio of bone minerals. However, the Ca/P ratios of the 'soaked in SBF for 15 days' scaffolds were changed over soaking period from their initial ratio of 6.28 (Ca/P ratio of as prepared scaffolds). EDS mapping for spatial elemental distribution of the soaked glass samples (Fig 6.4) was also in agreement with the HAp like layer formation on the scaffolds' surfaces.
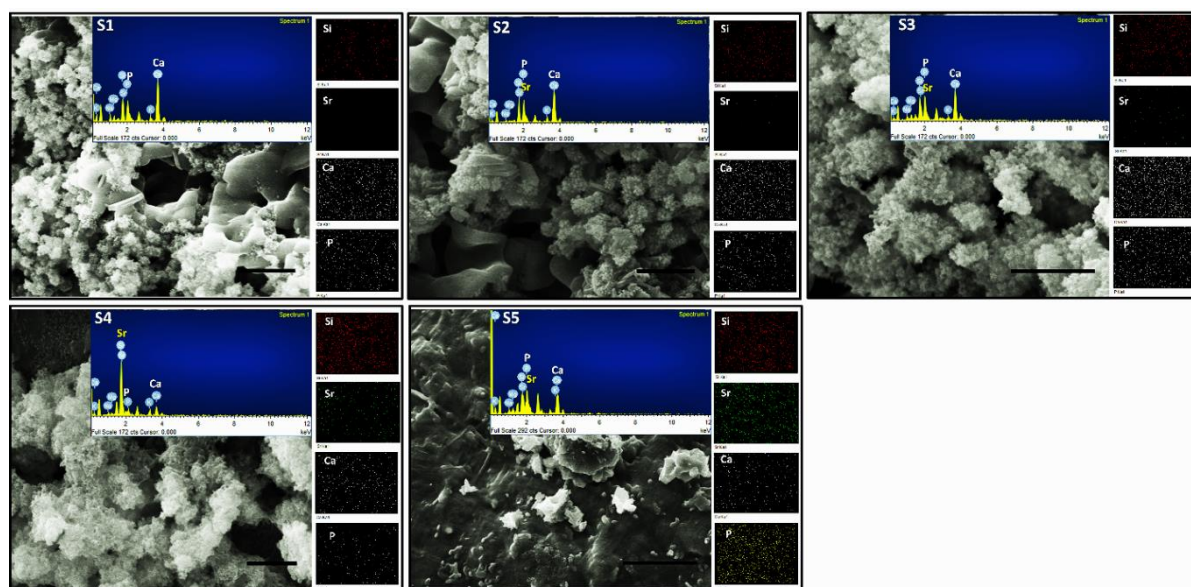

Fig 6.4 Surface morphology of the scaffolds after 15 days of immersion in SBF showing formation of HAp nodules. Energy Dispersive X-ray Spectroscopy (Inside) for elemental quantification showing elemental bands for Ca and P. EDS elemental mapping showing spatial distribution of Si, Ca, P and Sr elements. Inside bar=5µm.

Table 6.2: Theoretical (As prepared) concentration of Sr and Ca+Sr/P Vs EDS obtained concentration of Sr and Ca+Sr/P in the SrO derived 1393 glass scaffold

Scaffold	Theoretical value		EDS obtained value	
	Sr/Ca	Ca+Sr/P	Sr/Ca	Ca+Sr /P
S1	0	6.28	0	1.96
S2	0.053	6.28	0.039	1.62
S3	0.25	6.28	0.196	1.79
S4	1	6.28	0.841	1.65
S5	Undefined	6.28	3.3	1.47

6.4.2 In vitro cytocompatibility

6.4.2.1 Cellular metabolic activity, survivability and growth by MTT assay

Metabolic activity, survivability and growth after seeding L929 cells onto glass derived scaffolds (S1, S2, S3 and S5) and culture into complete medium for 1, 3 and 7 days were assessed via MTT and Live/ Dead assay. Scaffold-cells interactions in terms of cellular metabolic activity (OD at 570 nm) on day1 was found enhanced in S5 (0.127 ± 0; n=3) (Fig 6.5) than either of the pure (S1=0.05467 ± 0.00057; n=3) or other SrO derived (S2=0.082 ± 0, S3=0.04533 ± 0.0115) scaffolds. However, the absorbance on day3 was appeared preeminent in S1 (0.16833 ± 0.00057) followed by S5 (0.14667 ± 0.00153; n=3), S3 (0.12233 ± 0.00115; n=3) and S2 (0.104 ± 0.00346; n=3). Metabolic activity of the L929 cells over the scaffolds at 7th day was in anyway observed best in S2 (0.42 ± 0.002; n=3) than the other scaffolds (S1=0.398 ± 0, S3=0.279 ± 0.003 and S5= 0.25433 ± 0.00153).

Cellular viability was assessed through Live/Dead assay using cell-impermeant Calcein AM (green) and Ethidium homodimer-1 (red) stain for investigation of live (green) cells and dead (red) cells. Results (Fig 6.6) demonstrate that the live cells retained the Calcein AM on the surface and dead cells retained the Ethidium homodimer-1 stain within internal cells proteins after 24h co-culture with scaffold constructs. Visual inspection demonstrates better cellular survivability of L929 cells on the SrO derived scaffolds than that of the pure (1393) one.

Cell adhesion morphology (Fig 6.7) over the scaffolds' surface was examined by SEM after mouse fibroblast L929 cells were grown onto scaffolds for 2 weeks. Visual inspection from

the SEM micrographs clearly indicates that the dispersedly elongated cells over the scaffold constructs seemed adhered better in SrO derived scaffolds than that of the undoped one.
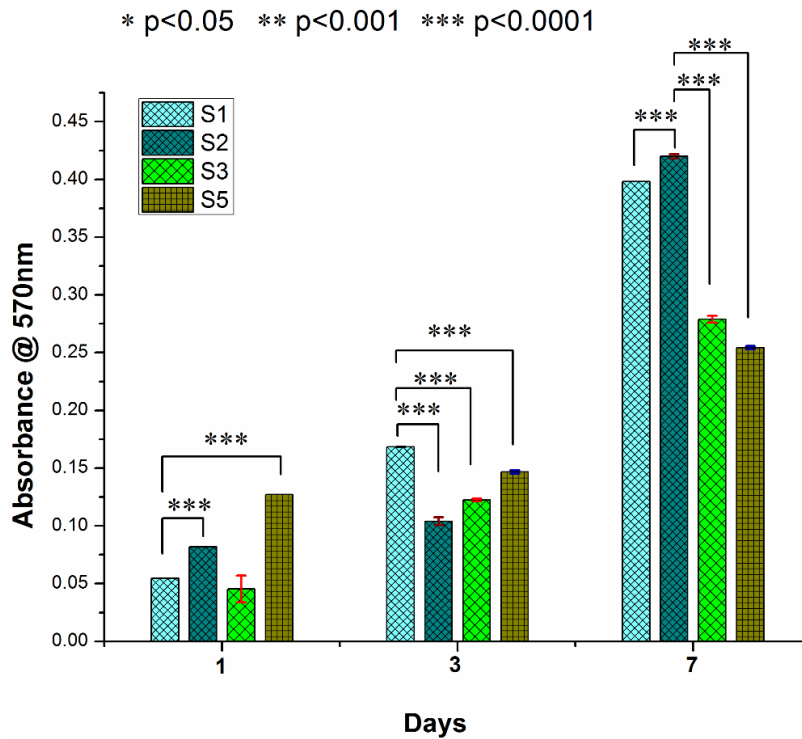

Fig 6.5 Cellular metabolism over the derived scaffolds. Statistical analysis of significance by one way ANOVA followed by Tukey's post hoc mean comparison considered significant (*) for p value <.05 and highly significant (**) for <.01 and p<.001 (n=3).
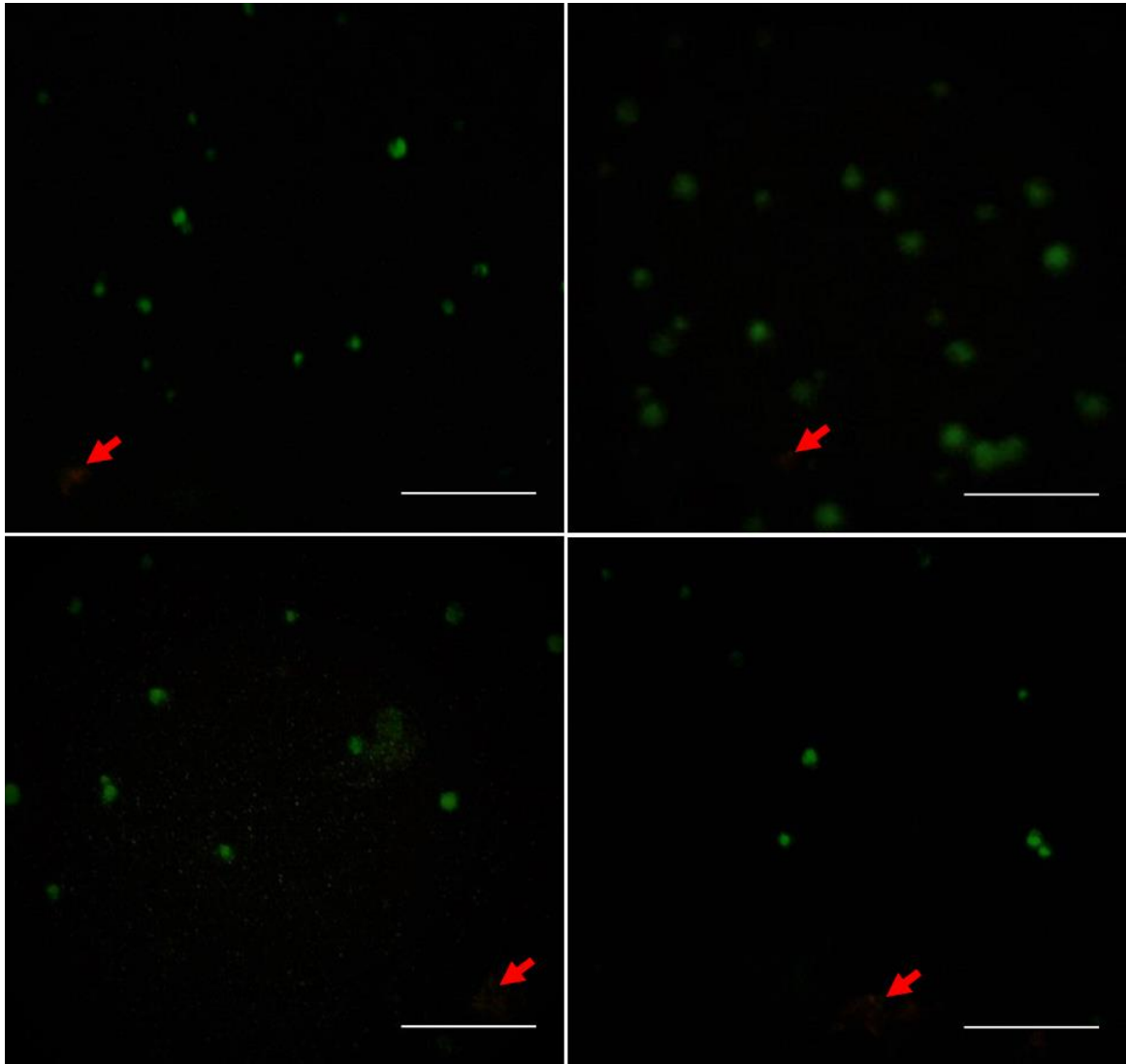
Fig 6.6 Cellular viability of murine fibroblast cells cultured onto scaffold constructs (S1-a, S2-b, S3-c and S5-d) using cell impermeant Calcein AM/ Ethidium homodimer-1 stain. Fluoresced images showing viable (Live; green) and apoptotic (Dead; red) cells (inside bar = 50µm).
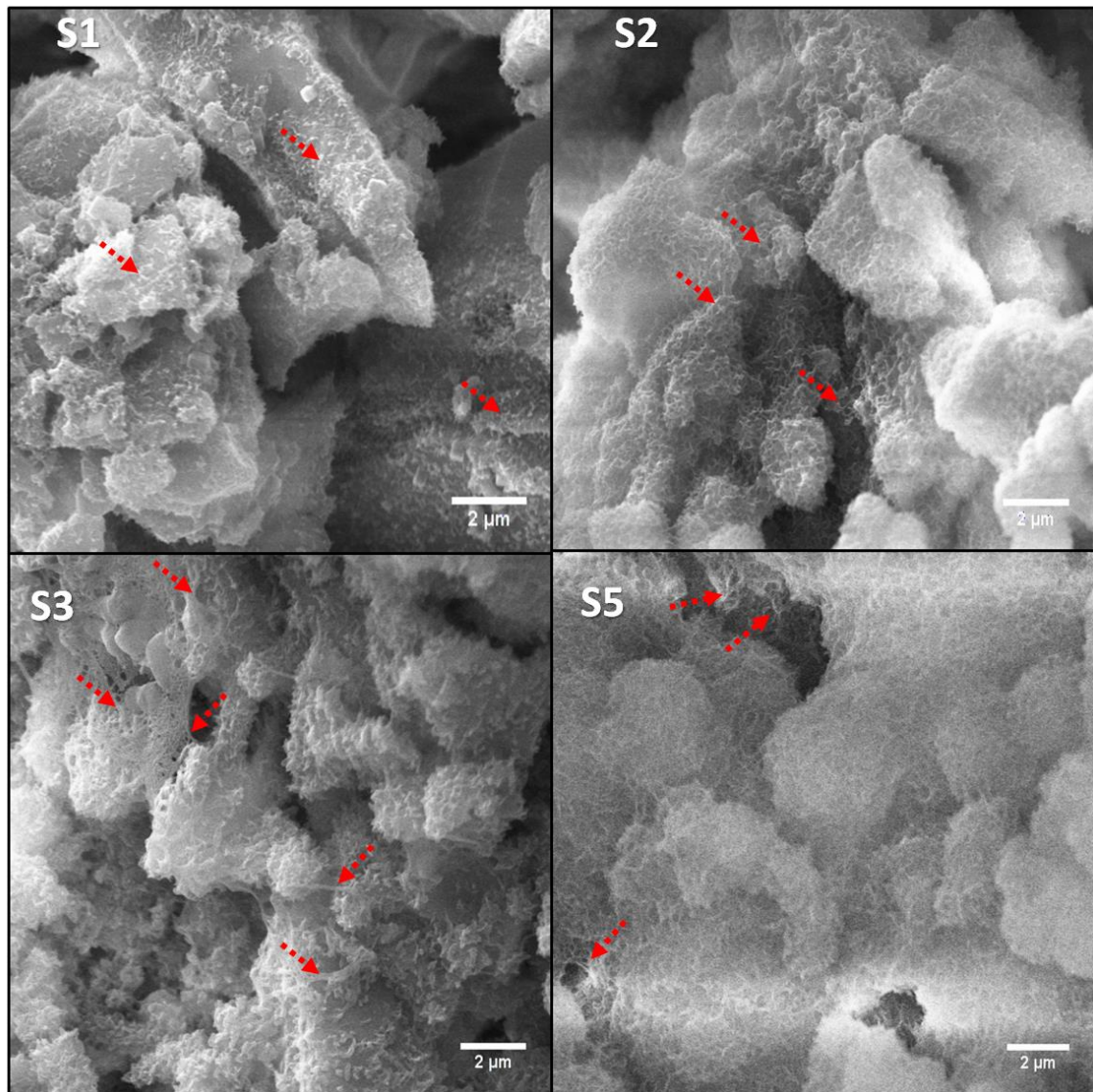
.

Fig 6.7 SEM micrographs of cell adhesion morphology over the scaffolds constructs after the murine fibroblast cells (L929) grown onto scaffolds for 24h. Red arrow showing elongated spindlier or irregular shaped cells attachment and spread over the glass surface

6.4.3 Mechanical properties

Three point bend (flexure) and compressive stress of the glass derived scaffolds of required dimensions (for flexural stress span length 25mm was fixed) were examined by subjecting under uniaxial 10 KN load cell of a UTM (Universal Testing Machine) (10KL, Tinius

Olsen, US) maintaining 0.05 mm/min cross head speed. The results indicate that the compressive stress was found to be increased with increasing SrO incorporation into the derived scaffolds. However, the compression data collected from the tests (Fig 6.8) were observed to be 11.2 ± 3.2, 12.7 ± 3.4, 16.4 ± 2.3, 13.8 ± 5.7, and 13.3 ± 2.7 MPa (n=3) for S1, S2, S3, S4 and S5 respectively (n=5). Further, the compression strengths of the scaffolds in wet condition after 2 weeks of immersion in SBF were also measured for cross examination of their mechanochemical stability in physiological fluid and the observed values were 5.9 ± 4.4, 7.7 ± 2.4, 10.5 ± 3.6, 9.2 ± 2.1 and 8.6 ± 2.9 MPa (n=3) respectively. Flexural stress of these scaffolds were also observed to be 1.22 ± 0.24, 1.17 ± 0.44, 1.89 ± 0.27, 1.63 ± 0.37 and 1.59 ± 0.27 MPa (in dry cond.) and 0.89 ± 0.21, 0.73 ± 0.54, 1.41 ± 0.31, 1.21 ± 0.27 and 1.15 ± 0.47 MPa (in wet cond.) respectively.

However, the apparent porosities of the sintered only scaffolds measured by solvent saturation method were appeared to be 53 ± 6.5, 49 ± 8.4, 52 ± 5.5, 47 ± 7.5 and 51 ± 4.5 for S1, S2, S3, S4 and S5 respectively. Additionally, the pore geometry of the surface morphological micrographs using NIH ImageJ software indicates that the scaffolds qualified the precondition of minimum pore radius for bone ingrowth by containing $> 50 \mu m$ pores (Loh and Choong, 2013).
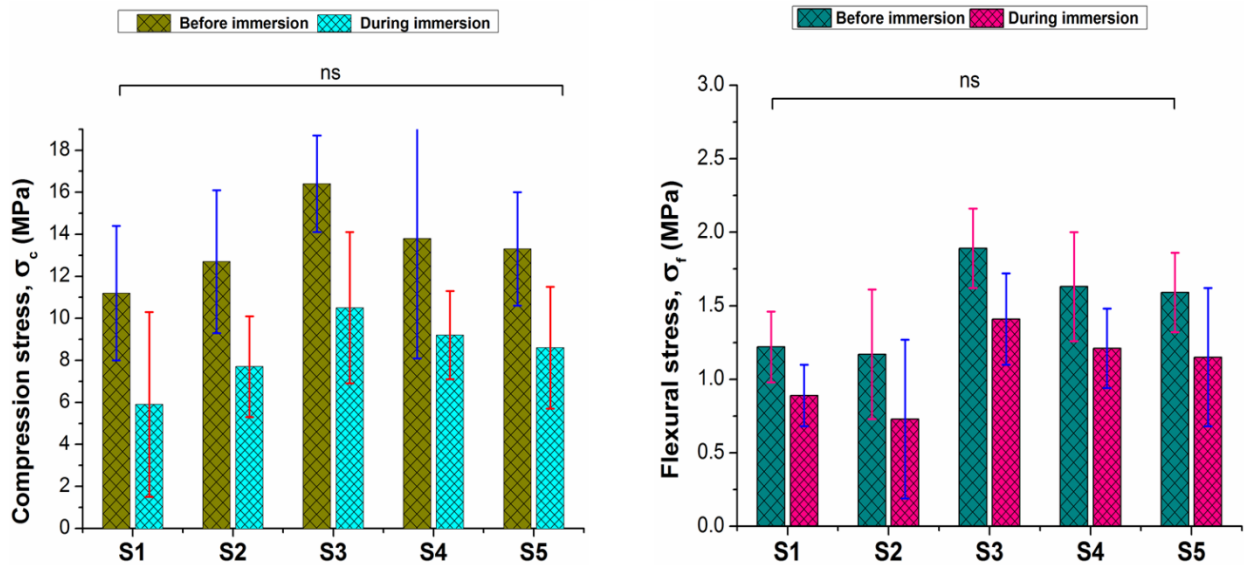
Fig 6.8 Compressive and flexural strengths of the scaffolds of as prepared and after immersion in simulated body fluid (wet condition). One way ANOVA with tukey's post hoc mean comparison considering significant difference for the $p < 0.05$; n=5.

6.5 Discussions

The In vitro bioactivity of materials is the measure of biocompatible surface mineralization (HAp crystals formation) ability in physiological condition. Herein, the HAp crystals formation as a measure of bioactivity was evaluated through morphological, structural and functional properties of materials and physico-chemical behavior of SBF solution (Ali et al., 2018, Ali et al., 2019, Vyas et al., 2016, Ershad et al., 2017, Ershad et al., 2018, Yadav et al., 2017, Yadav et al.). Here, in our observations of structural characterizations of 'soaked in SBF' scaffolds, the appearance of major crystalline peaks at 32°, 45° and 56° (2θ) were attributed to the HAp crystals formation matched with standard ICDD [PDF # 72-1243] (Ali et al., 2019). Evidently distinctive and exclusively explicit sharp crystalline peaks for soaked glass samples (Fig 6.1) supporting the proclamation of the evolution of HAp crystals on the scaffold surfaces. However, the evolution of HAp crystals during

soaking was supposed to have initiated through SBF mediated heterogeneous nucleation followed by the formation and growth of stable nuclei. The heterogeneous nucleation was mediated by SBF solution upon accumulation of Ca^{2+}, $PO_4{}^{3-}$ and $CO_3{}^{2-}$ species on the glass surfaces (Habraken et al., 2013). The rapid dissolution of ions from the glass surface and subsequent accumulation of specific ions on the silica rich layer formed an ACP (amorphous calcium phosphate) layer on the glass surfaces (Habraken et al., 2013, Yu et al., 2018). The pre-nucleation complexes on further accumulation converted to hydroxycarbonated apatite (HCA; $Ca_{10}(PO_4)_{6-y}(CO_3)_y(OH)_2$) (Kargozar et al., 2019, O'donnell and Hill, 2010, Kuda et al., 2018) layer via octacalcium phosphates (OCP; $Ca_8(HPO_4)_2(PO_4)_4.5H_2O$) (Ali et al., 2019, Habraken et al., 2013, Yu et al., 2018, Yun et al., 2018). However, the modification in calcium hydroxyapatite by other elements was also mentioned in our introduction part (Pilmane et al., 2017, Gomes et al., 2019). Partial to full substitution of SrO for CaO in 1393 glass scaffolds, the solid solutions of Sr-HCA were formed during soaking (O'Donnell et al., 2008). Further, the more pronounced peaks in the crystallographic spectra of the SrO derived scaffolds were noticed due to the formation of strontium apatite [Sr-HCA; $Ca_{(10-x)}Sr_x(PO_4)_{6-y}(CO_3)_y(OH)_2$](PDF # 72-1243, 33-1348) rather than calcium apatite (Fredholm et al., 2011). The increased intensities of strontium apatites in SrO derived glasses can be discussed as strontium being a heavy metal contains more electrons, therefore caused more constructive interference than calcium, henceforth more pronounced peaks than calcium apatite (O'Donnell et al., 2008). The other mild to moderate peaks for both the SBF treated and untreated samples were attributed to $Na_2Ca_{2-x}Sr_xO_9$ and or $Ca_{2-x}Sr_xSiO_4$ (Hesaraki et al., 2010, Fujikura et al., 2012).

Characterizations for functional groups through FTIR analysis (Fig 6.2) demonstrate various bending and stretching mode of vibrations representing PO_4 bands in soaked

samples. The spectral resonances at 1040 cm^{-1} can be assigned to stretching mode of PO$_4$ bands, which became intense over time due to the plausible superimposition of the preexisting Si-O-Si bands. The new or modified preexisting resonances at shorter wavenumber as described earlier were attributed to the bending mode of PO$_4$ bands. Presence of carbonyl and hydroxyl bands at 1100-1700 and 2700-3800 cm^{-1} over the spectral range was also confirmed for the soaked samples. No significant modifications other than some minor alterations in spectral characteristics were observed in SrO derived glass samples than the parent glass system.

Physicochemical pH behavior of the SBF solution, in common happens to increase abruptly (Fig 6.3A) for the initial few days (5 days in this case) of soaking due to rapid ion exchange between the surface cations (here Ca^{2+}, Sr^{2+}, Na$^+$, K$^+$ etc) and H$^+$ or H$_3$O$^+$ ions from the solution. Increased pH (basicity) of the solution attacks and dissolves the glass networks to form silanols (Si-OH). Then the alkali ions depleted silica rich layer was formed due to subsequent condensation and polymerization of hydrated silanols. Thereafter, the ACP formation occurred due to absorption of Ca^{2+}, $PO_4{}^{3-}$ and $CO_3{}^{2-}$ species on the glass surfaces (Ershad et al., 2017, Ershad et al., 2018, Yadav et al., 2017, Ali et al., 2018, Ali et al., 2019). The formation of ACP layer on the SiO$_2$ rich layer led to cut the connectivity between the scaffold surface and solution, thereby decreased pH after day5. Some alterations in physico-chemical behavior in SBF were also observed in SrO derived scaffolds in comparison to the pure 1393 (S1) glass scaffolds. The results (Fig 6.3A) demonstrate that the increase in SrO percentage in parent glass system have resulted in increase the pH of the simulated body fluid. Increase in pH for the SrO derived scaffolds can be evidenced owing to expansion in network structure due to entrance of larger Sr^{2+} cations (116pm) replacing smaller one (Ca=94pm). The expanded network due to their

increased interatomic bond length eventually made the whole glass structure slightly weaker, causing the ionic species to release at ease, and thereby enhanced the pH in the SrO derived samples. Being a network modifier, SrO incorporation into the glass system for any possible changes in bridging oxygen was further measured theoretically by the bellow glass network connectivity (NC) formula described elsewhere (O'donnell and Hill, 2010), considering SiO_2 alone formed the network structure while P_2O_5 remained in the orthophosphate phase.

$$NC = \frac{4 \times SiO_2 + 6 \times P_2O_5 - 2(Na_2O + K_2O + MgO + SrO + CaO)}{SiO_2}$$

This formula is however, claimed to be more applicable for melt-derived glasses, because sol gel glasses are supposed to contain residual content of hydrolysis silicate network. So according to the claim the NC of our derived scaffolds would be somewhat less than the obtained (2.59) value (O'donnell and Hill, 2010, Lao et al., 2009). The obtained calculated value for all of our glass samples would however, be unaltered even in fully substituted SrO for CaO in 1393 glass scaffold. Nevertheless, as higher pH of physiological fluid in SrO derived glasses have facilitated better HAp formation (Hench, 1991), indicating SrO incorporation in 1393 glass scaffold has enhanced the in vitro bioactivity of the glass samples.

Morphological study (Fig 6.4) indicates the formation of HAp nodules on the surface of the scaffold constructs for the entire set of glass samples. The formation of HAp layer was further confirmed by EDX elemental analysis (Ca/P ratio) and mapping through spatial distribution of elements.

The cells-scaffolds interactions by means of cellular metabolic activity (Fig 6.5) for the entire scaffolds were appeared to have augmented with the prolongation of culture

durations. Therefore, the results were clear indicating that the scaffolds were all biocompatibile, as none of them hindered the cellular metabolic activity during the whole culture period. In addition, the metabolic activity of the cells on both day1 and day7 was again found pronounced and significantly improved in S2, thereby indicating S2 (5 mol% SrO substitution for CaO in 1393) 'the most biocompatible' scaffold in comparison to the rest. The increase in metabolic activity in S2 can be attributed due to the formation of better biocompatible interface compared to S1, while S3 and S5 being observed creating higher pH microenvironment (Fig 6.2A) in physiological condition which could have affected the cellular metabolism of L929.

Nevertheless, the visual inspection of viable cells (Fig 6.6) by means of the Live/Dead assay was again seemed pronounced in S2 and least in cell lysis as well in comparison to either of pure (S1) or other SrO derived 1393 (S3 and S5) scaffolds. However, the cell adhesion (Fig 6.7) morphology over the scaffold constructs by SEM analysis gave somewhat different demonstration as opposed to Live/Dead or MTT assay. Herein, the visualized cell adhesion was seemingly increased with SrO substitution for CaO glass samples. The least attachment of murine fibroblast L929 cells was observed in S1. However, the cellular attachments were appeared significantly minimal for SrO derived scaffolds. Therefore, if taken altogether, S2 was the most cytocompatible scaffold studied by cell adhesion, MTT and Live/Dead assay.

The increased mechanical properties (Fig 6.8) for the SrO derived scaffolds was not completely understood. Strontium having larger cations (116pm) than calcium (94pm), their (SrO) substitution for CaO in the 1393 glass network could have resulted in expanding and weakening the overall network structure, thereby lessened the actual network strengths. Partial to full substitution of CaO by SrO in the derived glass by formation of solid solution

with expanded unit cells in the resultant crystallites was also in the agreement of increased pH of the SBF solution for the SrO derived scaffolds (Hill et al., 2004).

However, for the sintered only scaffolds the degree of crystallinity was appeared to have increased in the SrO derived samples. The increase in degree of crystallinity could be an indication of polymorphic transformation tendency of the SrO derived glasses into glass ceramics. As glass ceramics bear more arranged atomic order (cryptocrystalline) than normal glasses, their bond energy significantly improved, thus resulted in increased mechanical properties in SrO derived samples (Vyas et al., 2016). Further, the strontium being a heavy (atomic mass 87.62) and larger (116) element than calcium (atomic mass 40), their replacement could have enhanced compactness (closely packed) in the structure, and thereby enhanced the mechanical performance.

6.6 Conclusions

This investigation deals with the preparation of 3D porous scaffolds mimicking trabecular bone and their mechano-chemical and biological property evaluation. Despite having enough porosity (>50%) the SrO derived scaffolds showed compressive and flexural property close to that of trabecular bones. The bioactivity of SrO derived scaffolds comparing the pure glass system was also found enhanced due to formation of biocompatible Sr-HCA [$Ca_{(10-x)}Sr_x(PO_4)_{6-y}(CO_3)_y(OH)_2$] layer. Further, the Sr-HCA layer in SrO derived scaffolds has enhanced the cytocompatibility of L929 cells. Therefore, in conclusions, if taken altogether, the SrO derived 1393 scaffolds have shown some excellent bioactive, biocompatible and mechanical properties, and henceforth could be considered as potential future biomaterials for neo-bone tissue regenerative application.

<div align="center">ଔଃ౭</div>